Hindawi
International Journal of Antennas and Propagation
Volume 2021, Article ID 5368600, 13 pages
https://doi.org/10.1155/2021/5368600

*Research Article*

# Neural Network-Guided Sparse Recovery for Interrupted-Sampling Repeater Jamming Suppression

**Zijian Wang**,[1,2] **Wenbo Yu**,[1,2] **Zhongjun Yu**,[1,2] **Yunhua Luo**,[1] **and Jiamu Li**[1,2]

[1]*Aerospace Information Research Institute, Chinese Academy of Sciences, Beijing 100190, China*
[2]*School of Electronic, Electrical and Communication Engineering, University of Chinese Academy of Sciences, Beijing 101408, China*

Correspondence should be addressed to Zhongjun Yu; yuzj@ucas.ac.cn

Received 23 September 2021; Revised 8 November 2021; Accepted 16 November 2021; Published 2 December 2021

Academic Editor: Hervé Aubert



Interrupted-sampling repeater jamming (ISRJ) is a new type of DRFM-based jamming designed for linear frequency modulation (LFM) signals. By intercepting the radar signal slice and retransmitting it many times, ISRJ can obtain radar coherent processing gain so that multiple false target groups can be formed after pulse compression (PC). According to the distribution characteristic of the echo signal and the coherence of ISRJ to radar signal, a new method for ISRJ suppression is proposed in this study. In this method, the position of the real target is determined using a gated recurrent unit neural network (GRU-Net), and the real target can be, therefore, reconstructed by adaptive filtering in the sparse representation of the echo signal based on the target locating result. The reconstruction result contains only the real target, and the false target groups formed by ISRJ are suppressed completely. The target locating accuracy of the proposed GRU-Net can reach 92.75%. Simulations have proved the effectiveness of the proposed method.

## 1. Introduction

Linear frequency modulation (LFM) signal is widely used in wideband radar systems for its large time-bandwidth product and high Doppler tolerance [1, 2]. By coherent processing of LFM, noise jamming and other noncoherent jammings can be greatly suppressed. However, with the widespread application of digital radio frequency memory (DRFM) technology, a number of new types of radar jamming have been developed. DRFM has the ability to sample, store, modulate, and forward radar signals. By coherently replicating the radar signal, the generated jamming signal can retain the intrapulse modulation characteristic of the radar signal and can thus obtain the coherent processing gain at the radar receiver. Therefore, the application of DRFM has greatly reduced the transmission power requirement of the jammer, making it light enough to be loaded onto the target to flexibly interfere with the radar system.

Interrupted-sampling repeater jamming (ISRJ) is a newly proposed radar coherent jamming model based on DRFM [3]. By intercepting, delaying, and repeatedly forwarding the transmitted radar signal within a signal pulse width, a series of realistic coherent false target groups can be formed after range pulse compression (PC) [4]. The mathematical principle and performance of ISRJ are analyzed in [5]. On this basis, many researchers have analyzed and improved the jamming performance of ISRJ and have gradually applied ISRJ to jamming radar of various systems including synthetic aperture radar (SAR) and inverse synthetic aperture radar (ISAR) [6–11]. ISRJ can be adapted to both receive-transmit time-sharing antenna system and antenna system with two antennas working asynchronously [12]. Moreover, the instant sampling and forwarding process of ISRJ does not need to receive signals of complete signal duration, so the jammer can adjust parameters at any time to flexibly change the jamming mode, which poses a great threat to the radar system [13].

Nevertheless, the research studies on countering ISRJ are still lacking so far. The research study of ISRJ countermeasures mainly focuses on signal processing and waveform design. In terms of signal processing, for dechirping radar, a band-pass filter is designed [14] by using the discontinuity characteristic of ISRJ in the time-frequency (TF) domain. However, this method damages the continuity of the target signal in the frequency domain, resulting in strong sidelobe components of the PC result. In [15], the PC result of the echo signal is transformed into TF domain, and an adaptive filter is constructed to filter out ISRJ based on the discontinuity of false target in TF domain. A parameter estimation method using TF analysis and deconvolution of ISRJ is proposed in [16], and ISRJ is suppressed by interference cancellation through the reconstruction of the jamming signal. Based on signal sparse recovery, [17, 18] propose new ideas for jamming suppression. A wideband jamming suppression method based on TF domain filtering and sparse recovery is verified in [17]. In [18], the energy function is first used to extract the signal part not disturbed by ISRJ; then, the target reconstruction is completed based on the sparsity of the signal in the frequency domain after dechirping. In the aspect of waveform design, intrapulse frequency random coded signal is used in [19] to suppress the false target ahead of the real target generated by improved ISRJ through frequency modulation. In [20], a hybrid modulated signal is adapted to make the subpulses of the signal orthogonal to each other, and the real target is distinguished from the false target by subpulse compression.

Deep learning has recently shown excellent performance and broad application prospects in computer vision, speech recognition, natural language processing, and other fields. In terms of radar jamming suppression, due to the wide variety of radar signals and jamming models, how to make better use of deep learning methods has become the focus of research studies of scholars. Jamming suppression is regarded as an image processing problem in [21, 22]. First, the short-time Fourier transform (STFT) is applied to obtain the TF spectrum of the signal as the input of the convolutional network, and then, the jamming-free signal is output directly through the convolutional network. In [23], combined with the method of target detection, the author uses a single shot multibox detector (SSD) to detect the jamming signal in the TF domain and performs adaptive filtering according to the detected jamming types and jamming parameters to complete jamming suppression. For the dechirping radar system, a bidirectional gated recurrent unit (GRU) is used in [24] to classify signal segments in the time domain and filter out the part interfered by ISRJ. It can be seen that the current deep learning countermeasures against radar jamming are basically independent of traditional research studies, and the prior knowledge that may help the network understand the jamming model better is not fully utilized.

In this study, a method against ISRJ is proposed based on the coherence of ISRJ with respect to the real target signal and the different TF distribution characteristics between real target and false target groups. This method can reconstruct the real target through adaptive sparse filtering using the target locating result of the proposed GRU neural network (GRU-Net). The rest of this study is arranged as follows. Section 2 first introduces the signal model of the target signal and ISRJ and then analyzes the amplitude response and TF characteristics of the ISRJ PC result. Section 3 proposes the anti-ISRJ method based on GRU-Net target locating and sparse recovery. The process of real target locating using GRU-Net, sparse representation of the echo signal, and real target reconstruction is introduced. Section 4 conducts some simulations to validate the effectiveness of this method against ISRJ and studies the factors affecting the real target locating. Finally, the main conclusions are drawn in Section 5.

## 2. Principle of ISRJ

*2.1. Signal Model.* The LFM pulse radar transmits the LFM signal pulse by pulse and receives an echo signal from the target. Suppose that the target is equipped with an ISRJ jammer, the received echo signal will be polluted by ISRJ, which will seriously damage the imaging quality of the target and the subsequent detection.

Assume that the normalized LFM signal transmitted by radar is

$$s(t) = \mathrm{rect}\left(\frac{t - T_p/2}{T_p}\right) \cdot e^{j\pi k t^2}, \tag{1}$$

where

$$\mathrm{rect}\left(\frac{t}{T_p}\right) = \begin{cases} 1, & -\dfrac{T_p}{2} \le t \le \dfrac{T_p}{2}, \\ 0, & \text{else}, \end{cases} \tag{2}$$

represents a rectangular window of width $T_p$, $T_p$ is the pulse width of LFM signal, $k = B/T_p$ represents the chirp rate, and $B$ is the bandwidth of the LFM signal. The carrier frequency of the signal is omitted because it does not affect the derivation.

Assume that the distance between the target and the radar is $R_t$, the target echo signal received by the radar can be expressed by

$$s_t(t) = A_t s(t - \tau_t), \tag{3}$$

where $\tau_t = 2R_t/c$ represents the time delay of the target echo signal, $c$ is the speed of light, and $A_t$ is the amplitude of target echo signal, which can be calculated by radar equation.

The ISRJ jammer first intercepts and samples a slice of radar signal and then retransmits it many times. This process is repeated until the end of the radar pulse. Figure 1 shows the principle of ISRJ. $T_s$ is the repeat sampling interval, $T_I$ is the sampling pulse width, $M$ is the retransmission times of a single slice sampling, $T_s = (M+1)T_I$, $N$ is the number of radar signal slices that can be intercepted by the jammer within the duration of a radar signal pulse, and $N = T_p/T_s$.

The sampling equation $p(t) = \mathrm{rect}[(t - T_I)/T_I] * \sum_{n=0}^{N-1} \delta(t - nT_s)$ is a rectangular envelope pulse sequence with pulse width $T_I$ and pulse repetition interval PRT = $T_s$, where $*$ denotes convolution operator.

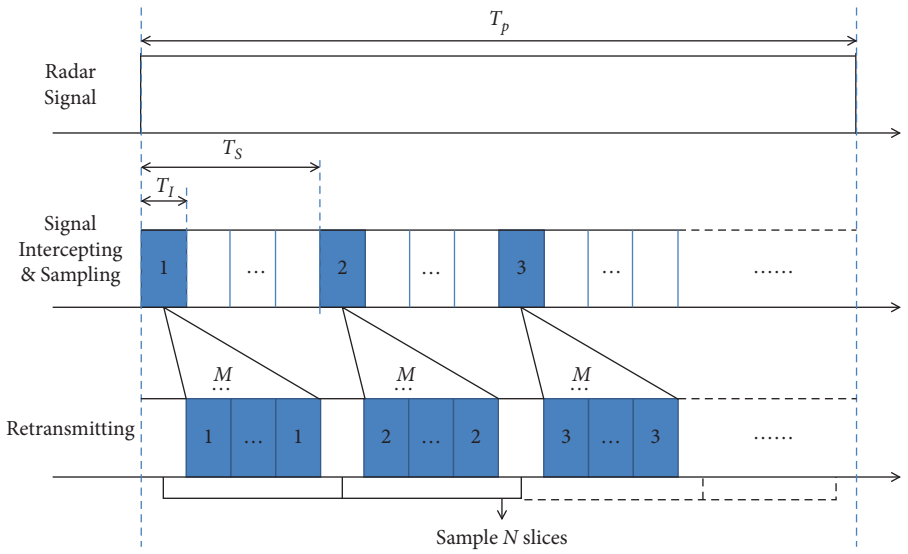


Figure 1: The principle of ISRJ.

Therefore, radar signals intercepted and sampled by jammers can be described by

$$x_s(t) = p(t-\tau_t)\cdot s(t-\tau_t) = \sum_{n=0}^{N-1} \mathrm{rect}\left(\frac{t - T_I/2 - \tau_t - nT_s}{T_I}\right)\cdot e^{j\pi k(t-\tau_t)^2}, \tag{4}$$

After intercepting and sampling the radar signal, the jammer retransmits the intercepted signal slice several times, and the resulting jamming signal can be obtained as follows:

$$\begin{aligned} J(t) &= A_j \sum_{m=1}^{M} x_s(t - mT_I) \\ &= A_j \sum_{m=1}^{M}\sum_{n=0}^{N-1} \mathrm{rect}\left(\frac{t - T_I/2 - \tau_t - nT_s - mT_I}{T_I}\right)\cdot e^{j\pi k(t-\tau_t-mT_I)^2}, \end{aligned} \tag{5}$$

where $A_j$ is the amplitude of the jamming signal, which can also be calculated by radar equation.

Finally, the echo signal received by radar includes target echo signal, jamming signal, and noise signal $n(t)$, which obeys a Gaussian distribution. The echo signal can be expressed by

$$\mathrm{Echo}(t) = s_t(t) + J(t) + n(t). \tag{6}$$

*2.2. PC Result of ISRJ.* The matched filter of LFM radar can be expressed as $s^*(-t)$. Taking the first retransmission of the $n$th jamming slice as an example (for convenience, the time delay is set at zero, which does not affect the results), the PC process can be regarded as the convolution between the matched filter and the jamming slice. With $T_I < T_p$, the PC result of that jamming slice is

$$
\begin{aligned}
PC_{n,1}(t) &= A_j \int_{-\infty}^{\infty} \mathrm{rect}\left(\frac{\gamma - T_I - nT_s}{T_I}\right)\mathrm{rect}\left(\frac{t-\gamma}{T_p}\right)\cdot e^{j\pi k(\gamma - T_I)^2}\cdot e^{-j\pi k(t-\gamma)^2}\,\mathrm{d}\gamma \\
&= A_j \int_{nT_s+T_I/2}^{nT_s+3T_I/2} e^{j\pi k\left[T_I^2 - t^2 + 2\gamma(t-T_I)\right]}\mathrm{d}\gamma \\
&= A_j e^{j\pi k\left(T_I^2 - t^2\right)}\cdot e^{j2\pi k(t-T_I)(nT_S+T_I)}\cdot \frac{e^{j\pi kT_I(t-T_I)} - e^{-j\pi kT_I(t-T_I)}}{j2\pi k(t-T_I)} \\
&= A_j T_I \frac{j2\,\sin\left[\pi kT_I(t-T_I)\right]}{j2\pi kT_I(t-T_I)} e^{j\varphi} \\
&= A_j T_I \mathrm{sinc}\left[kT_I(t-T_I)\right]e^{j\varphi},
\end{aligned}
\tag{7}
$$

where $\varphi = \pi k(T_I^2 - t^2) + 2\pi k(nT_s + T_I)(t - T_I)$. Equation (7) indicates that the PC result of that jamming slice is a "sinc" function with the peak value at $T_I$. Therefore, for the first retransmission of all jamming slices, the amplitude response of the PC result can be expressed by

$$
\begin{aligned}
\left|\mathrm{PC}_1(t)\right| &= \left|\mathrm{PC}_{0,1}(t)\cdot\sum_{n=0}^{N-1} e^{j2\pi k(t-T_I)nT_s}\right| \\
&= A_j T_I \left|\mathrm{sinc}\left[kT_I(t-T_I)\right]\frac{\sin\left[N\pi kT_s(t-T_I)\right]}{\sin\left[\pi kT_s(t-T_I)\right]}\right|.
\end{aligned}
\tag{8}
$$

The PC result of the same intercepted radar signal slice with different retransmission times only differs at time delay, so the amplitude response of the whole ISRJ PC result can be represented by

$$
\left|\mathrm{PC}(t)\right| = \sum_{m=1}^{M}\left|\mathrm{PC}_m(t)\right| = \sum_{m=1}^{M}\left|A_j T_I \mathrm{sinc}\left[kT_I(t-mT_I)\right]\frac{\sin\left[N\pi kT_s(t-mT_I)\right]}{\sin\left[\pi kT_s(t-mT_I)\right]}\right|. \tag{9}
$$

The above analysis shows that the amplitude response of the ISRJ PC result delay is a series of false target groups in the form of "sinc" with different delays. It mainly depends on some key parameters, such as $N$, $M$, $T_I$, and $A_j$.

*2.3. TF Analysis of PC Result.* The TF analysis can show the joint distribution of signal energy both in time and frequency domains. Generally, TF transformation is realized by STFT, which can be expressed as follows:

$$
\mathrm{STFT}(t, f, sig(t)) = \int_{-\infty}^{-\infty} \mathrm{sig}(t')\cdot \mathrm{win}(t'-t)\cdot e^{-j2\pi ft'}\,\mathrm{d}t', \tag{10}
$$

where $\mathrm{win}(t)$ is a sliding window function, and $\mathrm{sig}(t)$ is the input signal.

For the PC result of the echo signal, when a rectangular window is used, the TF distribution can be represented by

$$
\begin{aligned}
tf(\tau_s, f) &= \mathrm{STFT}\left(\tau_s, f, \mathrm{PC}_e(t)\right) \\
&= \int_{-\infty}^{\infty} \mathrm{rect}\left(\frac{t-\tau_s}{T_{\mathrm{win}}}\right)\cdot e^{-j2\pi ft}\cdot \mathrm{PC}_e(t)\mathrm{d}t,
\end{aligned}
\tag{11}
$$

where $\mathrm{PC}_e(t)$ is the PC result of the echo signal, $\tau_s$ is the sliding time, and $T_{\mathrm{win}}$ is the width of the sliding window. The TF distribution of $\mathrm{PC}_e(t)$ is shown in Figure 2.

As can be seen from Figure 2, the real target signal after PC presents a long and concentrated strip-shaped distribution in the TF domain, while the TF distribution of a certain jamming slice of ISRJ after PC is discontinuous in the TF domain and presents the form of "sinc" in the time domain and frequency domain, respectively. For jamming slices with the same retransmission time, the TF distribution is a series of "sinc" functions of the same time unit and different frequency units. For jamming slices intercepted from the same signal slice but with different retransmission times, the TF distribution can be expressed as multiple regularly distributed "sinc" functions of the same frequency unit and different time units.

To sum up, the ISRJ jammer intercepts and retransmits slices of the target echo signal, and each jamming slice corresponds to a single fragment that discontinuously distributes in the TF domain after PC, while the real target signal after PC presents a continuous strip distribution in the TF domain. Therefore, the real echo target and the false target groups

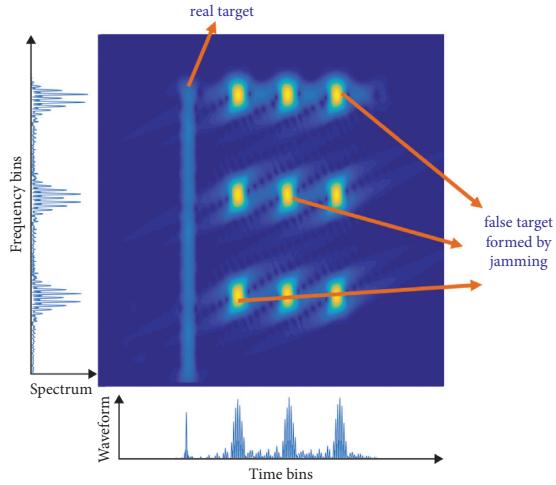


FIGURE 2: The PC result of the echo signal in TF domain, time domain, and frequency domain. The main graph shows the TF distribution of the PC result, the corresponding PC result in the time domain is shown below the main graph, and the corresponding PC result in the frequency domain is shown to the left of the main graph.

formed by ISRJ can be well distinguished after PC according to different distribution characteristics in the TF domain.

## 3. The Proposed Method

*3.1. Main Steps of the Proposed Method.* The TF distribution of ISRJ after PC is relatively short and discontinuous compared to the real echo target signal. Additionally, the distribution of different false target groups in the time domain is correlated among each other. In view of these characteristics, combined with GRU-Net, a new method against ISRJ is proposed in this study, the detailed process of which is listed in Algorithm 1.

*3.2. Real Target Locating Based on GRU-Net.* In order to accurately determine the time unit of the real target in the TF domain after PC, a gated recurrent unit neural network is proposed in this study. Stacked with two bidirectional GRU layers, GRU-Net can process the input data in both forward and backward directions along the time axis. Therefore, for the target locating task in this study, bidirectional GRU layers can make better use of distribution information of PC results and the correlation information between different time units compared with monodirectional GRU layers, thus locating the real target with less error probability.

The input of the GRU-Net is a normalized TF image of the echo signal after PC. The size of TF image is $N_r \times N_r$, where $N_r$ is the number of range sampling points. As the recurrent neural network is especially suitable for processing serialized data and further discovers the relationship among the internal elements of the sequence, the input TF image is regarded as a sequence signal along the time axis, where every column of the image $I$, a vector of length $N_r$, is one element of the sequence. The length of the sequence is $N_r$ accordingly. As shown in Figure 3, by extracting the features of these elements, GRU-Net can map the $t$th element $I_t$ to a single value $p_t$, which indicates the probability of column $t$ containing a target.

As shown in Table 1, an adaptive average pooling layer is applied at the beginning to reduce the dimension of input elements to a fixed size. Bidirectional GRU contains two independent GRUs working along with the opposite temporal directions, which are separately shown with blue and orange parts in Figure 3, so the output size is doubled compared to a single GRU. The output of GRU at the $t$th time unit $o_t$ depends both on the input at the $t$th time unit $i_t$ and the last hidden state $h_{t-1}$, so we input the down-sampled element step by step. After two GRU layers, a linear layer takes the output vector of GRU2 as input and outputs a single value $p_t$ at each time unit. In the end, softmax is applied along the time axis to normalize $p_t$, and the final target location can be obtained by

$$r_t = \underset{t\in\{1,2,3,\ldots,N_r\}}{\operatorname{argmax}} \tilde{p}_t, \tag{12}$$

where $\tilde{p}_t$ is the normalized $p_t$.

*3.3. Sparse Recovery of Target Echo Signal.* Since the generation process of ISRJ is intercepting, sampling, and delayed forwarding of the radar target signal, each ISRJ slice is equivalent to a target echo signal with smaller pulse width. Therefore, based on the coherence of ISRJ relative to the target echo signal, the echo signal can be represented by the dictionary, which is constructed by the target echo signal.

$$\text{Echo}(t) = s_t(t) + J(t) + n(t) = D\sigma_1 + n(t), \tag{13}$$

where $D$ is the dictionary of sparse representation, which is a $N_r \times L$ matrix, $N_r$ is the number of sampling points in range direction, and $L$ is the number of range gates. Each column of the dictionary is a delayed form of transmitting signal, and different column corresponds to different time delay. The specific form of the dictionary can be expressed as

$$D = [s(t)s(t-\Delta\tau)s(t-2\Delta\tau)\cdots], \tag{14}$$

**Input:** The echo signal Echo$(t)$, the sliding window win$(t)$, the trained GRU-Net, the dictionary $D$.
**Output:** Target locating result $r_t$, the reconstructed target echo signal $\hat{s}_t$
**Begin**
(1) Perform pulse compression of Echo$(t)$;
(2) Implement STFT to transform the PC result PC$_e(t)$ into TF domain;
(3) Normalize the TF data;
(4) Input the normalized TF data into the GRU-Net;
(5) Obtain the GRU-Net target locating result $r_t$;
(6) Carry out the sparse representation $\hat{\sigma}_1$ for Echo$(t)$;
(7) Construct an adaptive filter *Filter* according to $r_t$ to filter out the corresponding peaks of the false target groups in the sparse representation domain;
(8) Reconstruct the target echo signal $\hat{s}_t$ through $D$ and amplitude compensation to obtain the jamming-free result;
**End**

Algorithm 1: The proposed method.

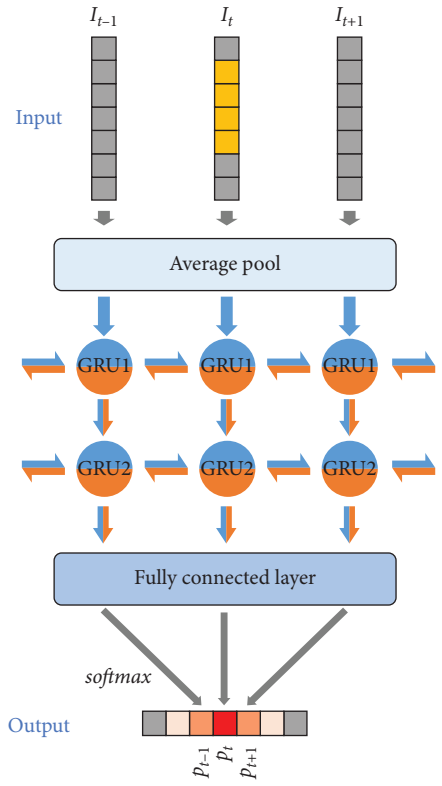


Figure 3: Pipeline of the proposed GRU-Net. The network is stacked by an average pooling layer, two bidirectional GRU layers, and a fully connected layer.

where $\Delta\tau$ is the time delay between two adjacent columns, and the range resolution of sparse representation is $\Delta R = \Delta\tau \cdot c$. $\sigma_1$ is a $L \times 1$ vector representing the energy factor of the real target and the false targets generated by ISRJ. When the real target distributes sparsely in the range domain, the false target groups formed by intercepting and retransmitting the real target signal can also be considered as sparsely distributed in the range domain. $\sigma_1$ has only several nonzero coefficients on the corresponding range gate of the real target and main false targets generated by ISRJ. The echo signal, therefore, has a sparse representation using the above dictionary.

The sparse representation can be obtained by solving the following convex optimization equation:

$$\min_{\sigma_1} \left\| \text{echo}(t) - D\sigma_1 \right\|_2^2 + \lambda \left\| \sigma_1 \right\|_1, \tag{15}$$

where $\|\cdot\|_p$ is the $l_p$ norm, and the non-negative coefficient $\lambda$ is used as a trade-off factor to compromise the sparsity $\|\hat{\sigma}_1\|_1$ and residual $\hat{r} = \text{echo}(t) - D\hat{\sigma}_1$ of the optimization solution $\hat{\sigma}_1$ of this equation. The larger the $\lambda$ is, the sparser the $\hat{\sigma}_1$, but the residual will also be correspondingly larger. The sparse representation of the echo signal is shown in Figure 4.

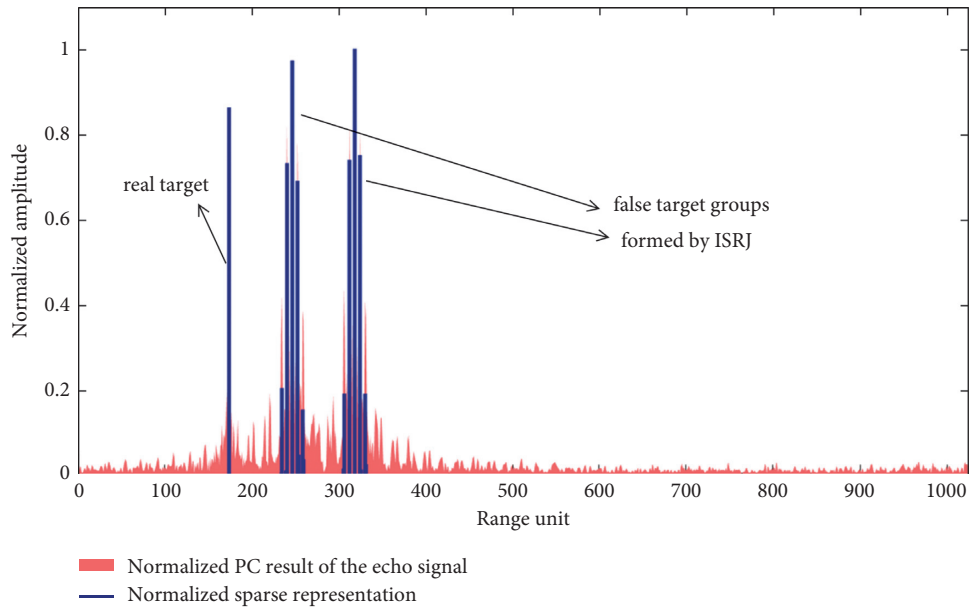


FIGURE 4: Sparse representation of echo signal. The blue line demonstrates the sparse representation result of the echo signal, and the red part shows the corresponding PC result. There are two false target groups, which means the retransmission time $M = 2$.

As can be seen from Figure 5, noise is greatly suppressed in the process of solving Equation (15). Because the real target echo signal and ISRJ are consistent with the dictionary, peaks can be generated at the positions corresponding to the real target and the main false target groups, and the height of the peaks represents the corresponding energy.

According to the sparse representation of the echo signal and the target locating result of GRU-Net, an adaptive filter can be constructed in the sparse representation domain to filter out the peaks of false targets and retain the peak of the real target, which can be represented by

$$\text{Filter} = [\, e_1 \;\; e_2 \;\; \cdots \;\; e_L \,], \tag{16}$$

where

$$e_i = \begin{cases} 1, & i = r_t, \\ 0, & \text{else}, \end{cases}, \quad t = 1, 2, 3, \ldots, L \tag{17}$$

Then, the reconstructed target echo signal can be expressed by

$$\hat{s}_t = \varepsilon\, D\sigma_{\text{opt}} = \varepsilon\, D\hat{\sigma}_1 \cdot \text{Filter}, \tag{18}$$

where $\varepsilon$ is the amplitude compensation factor, which is the ratio of the target amplitude before jamming suppression to the reconstructed target amplitude. Through multiplying the PC result of the reconstructed signal by $\varepsilon$, the final signal reconstruction result where ISRJ and noise are greatly suppressed can be obtained.

## 4. Simulations

*4.1. Data Training.* The proposed method can accurately reconstruct the target signal if the real target position is correctly located, which is regarded as successful antijamming. Therefore, the performance of the proposed method depends on the target locating precision of GRU-Net, which can be expressed by

$$P_s = \frac{N_c}{N_t}, \tag{19}$$

where $N_c$ is the number of correct locating samples, and $N_t$ is the total number of samples.

The proposed GRU-Net is trained by supervised learning. In order to obtain an accurate target position, 4,000 groups of simulated echo signals with random parameters are generated, which are divided into the training set, validation set, and test set in accordance with the ratio of 8 : 1 : 1. The parameter ranges of training samples are listed in Table 2.

Since the task for GRU-Net is more like a multi-classification problem, we choose one-hot encoding as our training label, which can be denoted as

$$y_t = \begin{cases} 1, & t = t_{\text{tar}}, \\ 0, & \text{else}, \end{cases}, \quad t = 1, 2, 3, \ldots, N_r, \tag{20}$$

where $t_{\text{tar}}$ is the position of the real target.

The network is optimized by the stochastic gradient descent (SGD) optimization algorithm based on a weighted cross-entropy loss, i.e., as follows:

$$\text{Loss} = -\sum_{t=1}^{N_r} [\, y_t \ln(p_t) + \beta(1 - y_t)\ln(1 - y_t)\,] e^{l^2}, \tag{21}$$

where $y_t$ is the corresponding target label. Weight $\beta$ is a hyperparameter designed to balance the importance of

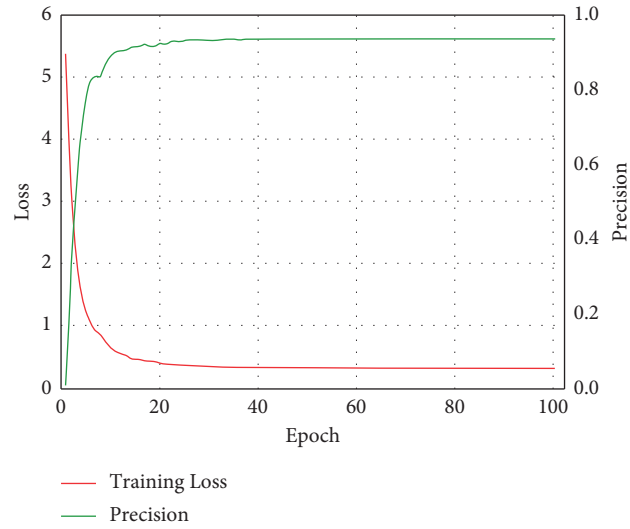


Figure 5: Training process curves. The red and green lines denote loss value and target locating precision, respectively.

Table 1: Structure of the proposed GRU-Net

| Layer | Output shape | Params num |
|---|---|---|
| Input placeholder | $[N_r, N_r]$ | 0 |
| Average pooling | $[N_r, 128]$ | 0 |
| Bidirectional GRU1 | $[N_r, 32 * 2]$ | 31104 |
| Bidirectional GRU2 | $[N_r, 16 * 2]$ | 7872 |
| Linear + softmax | $[N_r, 1]$ | 33 |

positive/negative examples, which is set to 0.001 in our experiments.

In the optimization process, the network is trained for 100 epochs with a total of 128 samples per minibatch. The initial learning rate is set to 0.0001, with momentum of 0.9 and weight decay of 0.0005. To check the convergence property of the proposed GRU-Net, the curve of loss value and target locating precision versus the number of training epochs is shown in Figure 5 by a red line and a green line, respectively. It can be seen that the training loss decreases rapidly with the increase in training rounds while the detection accuracy of the real target position continues to rise, and they both remain stable in the end. After training for 100 epochs, the final target locating precision stays at 92.75%.

In order to prove the advantages of the proposed GRU-Net, we construct a LSTM-Net by replacing the GRU layers of GRU-Net with LSTM layers under the condition that the network structure and training hyperparameter remain unchanged, and a contrast experiment is carried out to compare the target locating precision between the two networks. Experimental result shows that after training for 100 epochs, the target locating precision $P_s$ of both neural networks is maintained at 92.75%. However, the model size of LSTM-Net is 206 kB, while the model size of GRU-Net is 155 kB, which means that GRU-Net has a lower computational burden compared to LSTM-Net, while the target locating performance of the two neural networks is very close to each other.

A hypothesis test can verify the stability and excellence of the proposed network [25]. To further prove the advantage of GRU-Net in the target locating task, we perform a one-tailed $t$-test on the generated dataset, and the intermediate result of the statistical hypothesis calculation process is listed in Table 3. The target locating precision $P_s$ is taken as an evaluation matrix in the $t$-test. It can be seen from Table 3 that the average test $P_s$ value of GRU-Net is $\mu = (1/m_1)\sum_{s=1}^{m_1} \widehat{\varepsilon_s} = 0.9217$, and the variance is $\sigma^2 = [1/(m_1 - 1)]\sum_{s=1}^{m_1} (\widehat{\varepsilon_s} - \mu)^2 = 1.9167 \times 10^{-5}\,(m_1 = 6)$.

Finally, the critical value $\tau_t$ can be obtained by $\tau_t = \sqrt{m_1}|\mu - \varepsilon_0|/\sigma = 3.730$ (where $\varepsilon_0$ is the assumed minimum $P_s$ value, and $\varepsilon_0 = 0.915$). The critical value $\tau_t$ is larger than the given value of 3.365 by the one-tailed $t$-test table, which means that the test $P_s$ value of GRU-Net is larger than the assumed test $P_s$ value (0.915) with a confidence degree of $(1 - \alpha = 0.99)$.

*4.2. Factors Affecting Target Locating Precision.* Since the target locating precision is highly correlated with the input TF data, we consider that the target locating precision may be related to the signal-to-noise ratio (SNR), jamming-to-signal ratio (JSR), and $T_I$ of the echo signal. Among them, SNR and JSR represent the power ratio of signal to noise and interference to signal, respectively, which can be defined as

Table 2: Parameter ranges of training samples

| Parameter | Value |
|---|---|
| Sampling frequency $f_s$/MHz | 20 |
| Pulse width $T_p/\mu$s | 20–30 |
| Bandwidth $B$/MHz | 6–10 |
| Target range $R$/km | 5–15 |
| Repeat sampling interval $T_s/\mu$s | 5–12 |
| Retransmission time $M$ | {1, 2, 3, 4} |
| Signal-to-noise ratio SNR/dB | −10 to 10 |
| Jamming-to-signal ratio JSR/dB | 5–20 |

Table 3: Hypothesis test of GRU-Net on the generated dataset

| Statistical parameter | Value |
|---|---|
| $\mu$ | 0.9217 |
| $\varepsilon_0$ | 0.915 |
| $\sigma^2$ | $1.9167 \times 10^{-5}$ |
| $\tau_t$ | 3.730 |
| $1-\alpha$ | 0.99 |

$$\begin{cases} \text{SNR} = 10\lg\left(\dfrac{A_t^2}{\sigma_n^2}\right), \\ \text{JSR} = 10\lg\left(\dfrac{A_j^2}{A_t^2}\right), \end{cases} \tag{22}$$

where $\sigma_n{}^2$ denotes noise power.

In order to study the effect of SNR and JNR on target locating precision, a series of Monte Carlo simulations are carried out in this study. The generated test sets are divided into 8 modes with different retransmission times $M$ and a number of jamming slices $N$. The settings of these eight modes are shown below in Figure 6. In the Monte Carlo simulations, the test sets are generated from 5 dB to 20 dB at 3 dB JSR intervals and from -10 dB to 10 dB at 5 dB SNR intervals, respectively. This results in 30 test groups per mode, and 100 Monte Carlo simulations are conducted in every test group.

In consideration of controlling variables, the bandwidth $B$ and the pulse width $T_p$ of the target echo signal are set at 9 MHz and 26 $\mu$s, respectively. The repeated sampling interval $T_s$ is separately set at 0.26 $T_p$ and 0.39 $T_p$, corresponding to two different numbers of jamming slices $N$. Other parameters remain the same as those listed in Table 1.

When $M = 1$, it means that the jammer intercepts a slice of the radar signal and directly retransmits the intercepted slice once. At this time, the jamming signal is called interrupted-sampling direct jamming (ISDJ), which differs from ISRJ only in the retransmission time of jamming slices. According to Section 2, the TF distribution of false target groups after PC is discontinuous compared with the real target, but there are only few correlations in the range domain because there is only one false target group.

The changing trend of target locating precision $P_s$ in 8 modes of ISRJ and ISDJ versus JSR and SNR is shown in Figure 7. Some key conclusions can be drawn from Figure 7, which are shown in the following:

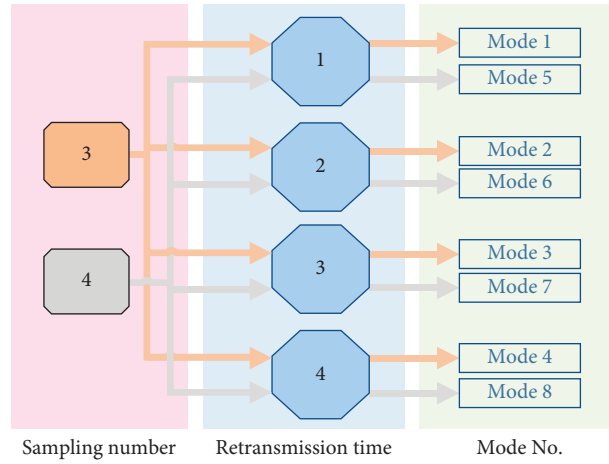


Figure 6: The setting of eight modes.

(1) In the case of fixed JSR, $P_s$ increases with the increase in SNR in the same mode.

(2) When SNR is small, target locating is relatively prone to error, but the changing trend of $P_s$ is not obvious versus JSR. In general, a larger JSR has a greater negative impact on $P_s$.

(3) When the retransmission time $M$ is fixed, the more the sampling numbers of the signal, the more chaotic the TF distribution of the echo after PC, and the $P_s$, in general, is relatively low.

(4) The TF distribution of the echo after PC is chaotic when the sampling number $N$ and the retransmission time $M$ are large (see mode 4 and mode 8), which is, in general, unfavorable for target locating.

(5) It can be seen that GRU-Net not only has an excellent performance in target locating in the case of ISRJ but also can realize target locating based only on the distribution difference in the TF domain between real target and false target groups in the case of ISDJ, which means that the proposed method has the ability to suppress not only ISRJ but also ISDJ.

According to Equation (9), when the sampling number $N$ and retransmission time $M$ are fixed, the TF distribution of ISRJ after PC is mainly related to $T_I$. For the purpose of learning the specific impact of $T_I$ on $P_s$, 1,000 test data are generated with $N$ and $M$ fixed at 4, and $T_I$ is uniformly distributed in the interval of $1.35 \sim 1.80\,\mu$s. The mislocated data are statistically analyzed, and the statistical result is shown in Figure 8. It can be seen that when $T_I$ is smaller, despite that the amplitude of false targets is smaller, the false target groups are more densely distributed in the range domain, which may result in lower target locating precision.

*4.3. The Jamming Suppression Performance of the Proposed Method.* In view of the fact that the proposed GRU-Net can achieve high target locating precision under ISRJ, the jamming suppression performance of the proposed method

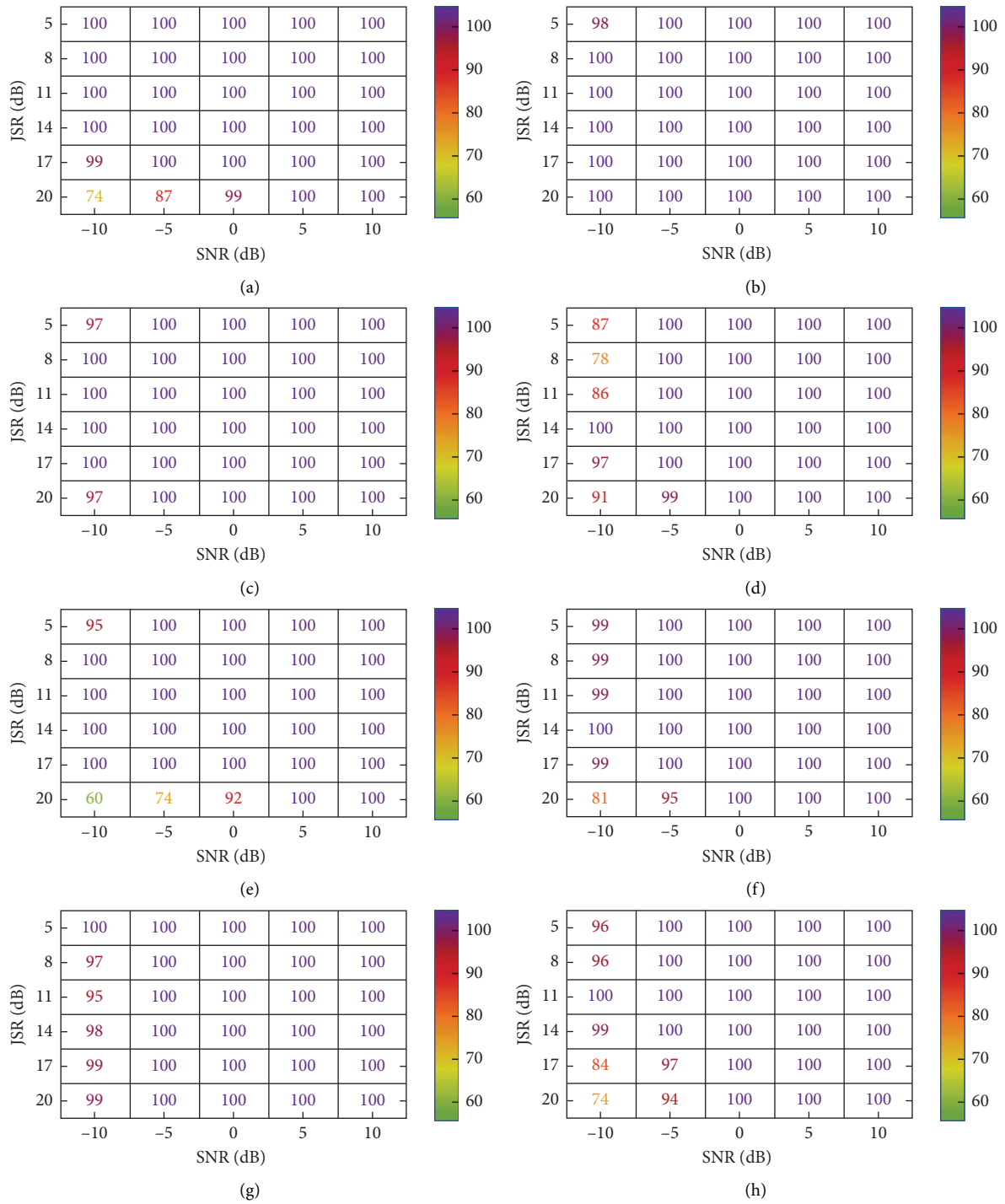


Figure 7: $P_s$ versus SNR and SJR. (a) Mode 1. (b) Mode 2. (c) Mode 3. (d) Mode 4. (e) Mode 5. (f) Mode 6. (g) Mode 7. (h) Mode 8.

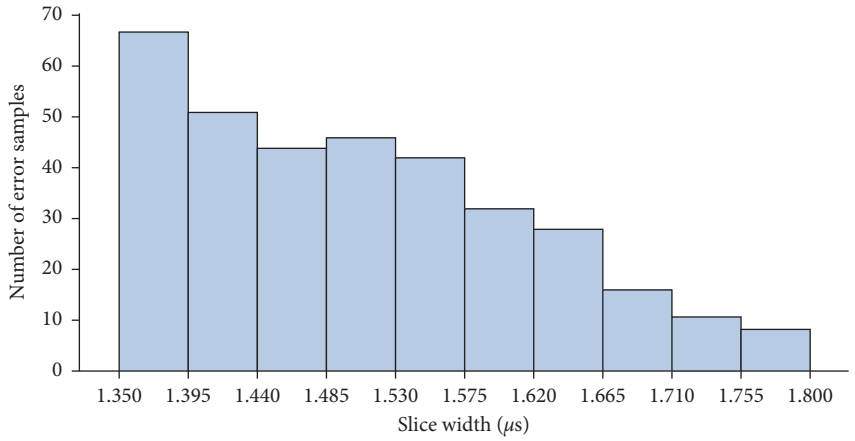


Figure 8: $T_I$ distribution of error samples.

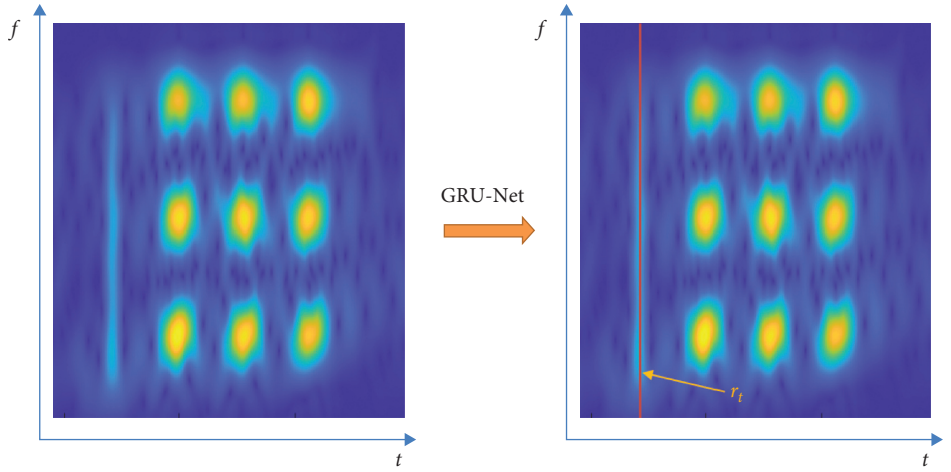


Figure 9: Target locating result by GRU-Net.

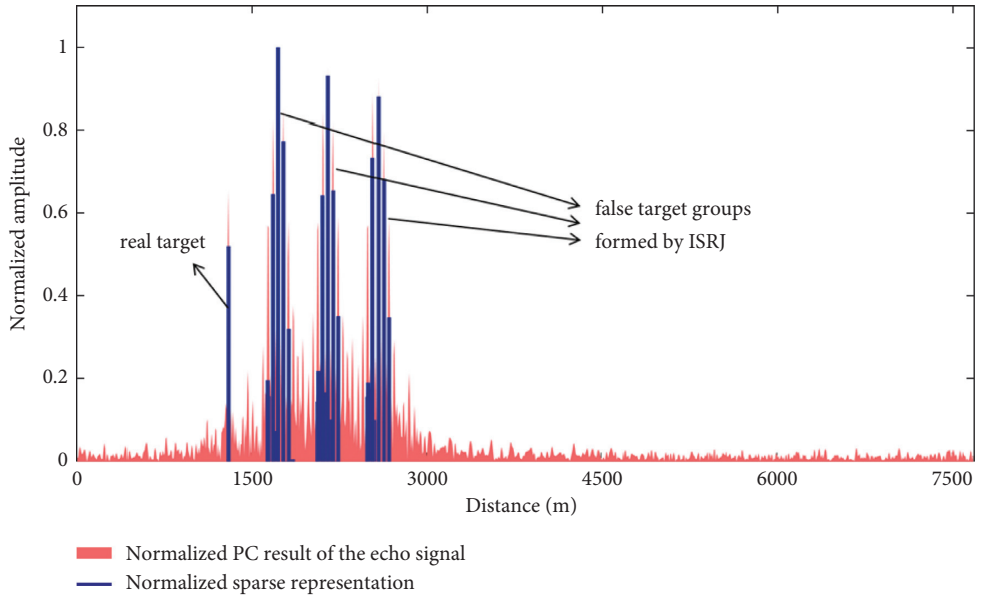


Figure 10: Spare representation of the echo signal. There are three false target groups, which means the retransmission time $M = 3$.

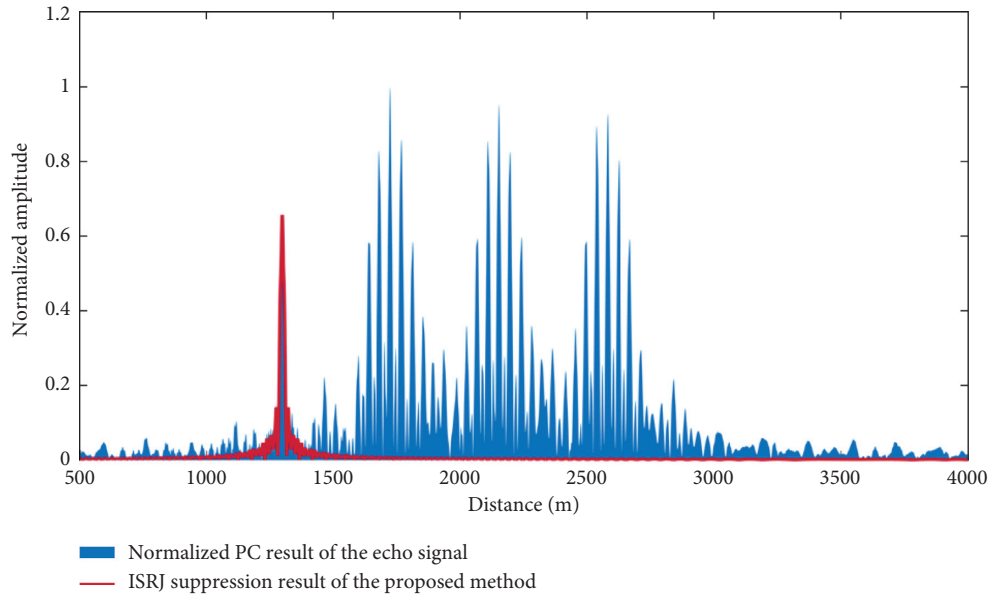


Figure 11: ISRJ suppression result of the proposed method.

is, therefore, tested. The bandwidth $B$ and the pulse width $T_p$ of the target echo signal are set at 9 MHz and 30 $\mu$s, respectively. The repeated sampling interval $T_s$ is set at 0.38 $T_p$, and the intercepted radar signal slice is retransmitted three times. The real target position is at 1,300 m. Under the condition that SNR is 5 dB and JSR is 15 dB, the TF data of the echo signal are first input into the proposed GRU-Net, and the actual position of the real target can be acquired, which is shown in Figure 9.

On the other hand, this echo signal is sparsely represented, and the result is shown in Figure 10. It can be seen from the result of sparse representation that there are three false target groups formed by retransmission, and the amplitude of main false targets in each false target decreases rapidly from the middle to the two sides.

According to Equation (17), an adaptive filter is constructed based on the target locating result by GRU-Net. After sparse domain filtering and amplitude compensation, the target signal is reconstructed, and the final jamming suppression result is obtained, which is shown in Figure 11. It can be seen that the proposed method successfully suppressed ISRJ and noise after signal reconstruction.

## 5. Conclusions

Based on the distribution characteristic of the echo signal and the coherence of ISRJ with respect to the radar signal, an ISRJ suppression method using sparse representation and deep learning target locating is innovatively proposed in this study. First, the TF domain data of the echo signal after PC are input into the proposed GRU-Net, and the location of the real target can be acquired according to the different TF distribution characteristics and the correlation information between the false target groups formed by ISRJ and the real target. Then, the coherence of the target signal and ISRJ relative to the constructed dictionary is used to sparsely represent the received echo signal. As a result, there are peaks at the exact range position of the real target and the strong false target groups, and the real target is, therefore, reconstructed after filtering in the sparse domain to achieve ISRJ suppression. Simulation results have demonstrated the effectiveness of the proposed method.

Because of the noncoherence between the noise signal and the constructed dictionary, the noise signal is also greatly suppressed besides ISRJ. The method proposed in this study is not limited to the suppression of ISRJ. For other kinds of sliced forwarding jammings with different forwarding modes or different modulation modes, they forward or modulate slices of radar signal so that the generated jamming signal is discontinuous both in the time domain and frequency domain compared with radar signal. Based on this characteristic, the proposed method can also be used to distinguish the real targets from the false targets in the TF domain under these types of jammings. Therefore, the proposed method also has great reference significance for the suppression of other DRFM-based slice forwarding jammings.

## Data Availability

The data of Monte Carlo simulations used to support the findings of this study are available from the corresponding author upon request.

## Conflicts of Interest

The authors declare that there are no conflicts of interest regarding the publication of this paper.

## References

[1] S. Baher Safa Hanbali, "Technique to counter improved active echo cancellation based on ISRJ with frequency shifting," *IEEE Sensors Journal*, vol. 19, no. 20, pp. 9194–9199, 2019.

[2] C. Liu, S. Liu, C. Zhang, Y. Huang, and H. Wang, "Multipath propagation analysis and ghost target removal for FMCW automotive radars," in *Proceedings of the 2020 IET International Radar Conference (IRC)*, pp. 1–5, Chongqing, China, November 2020.

[3] M. J. Sparrow and J. Cikalo, "ECM techniques to counter pulse compression radar," United States Patent, 7081846, 2006.

[4] D. C. Schleher, *Electronic Warfare in the Information Age*, Artech House, Boston, MA, USA, 1999.

[5] X. Wang, J. Liu, and W. Zhang, "Mathematic principles of interrupted-sampling repeater jamming (ISRJ)," *Electronic Warfare in the Information Age Science in China Series F: Information Sciences*, vol. 50, no. 1, pp. 113–123, 2007.

[6] D. Feng, L. Xu, X. Pan, and X. Wang, "Jamming wideband radar using interrupted-sampling repeater," *IEEE Transactions on Aerospace and Electronic Systems*, vol. 53, no. 3, pp. 1341–1354, 2017.

[7] D. Feng, H. Tao, Y. Yang, and Z. Liu, "Jamming de-chirping radar using interrupted-sampling repeater," *Science in China Series F: information Science*, vol. 54, no. 10, pp. 2138–2146, 2011.

[8] X. Pan, W. Wang, D. Feng, and Y. Liu, "On deception jamming for countering bistatic ISAR based on sub-Nyquist sampling," *Radar Sonar & Navigation*, vol. 8, no. 3, pp. 173–179, 2014.

[9] G. Liu, K. Zheng, and M. Gao, "Design and implementation of deception jamming signal generator against SAR," *Transactions of Beijing Institute of Technology*, vol. 32, no. 2, pp. 184–188, 2012, Chinese.

[10] W. Yang, J. Lin, and T. Wang, "Intermittent sampling scatterwave jamming against SAR," *Journal of Astronautics*, vol. 3, no. 33, pp. 367–373, 2012, Chinese.

[11] C. Li, W. Su, G. Hong, C. Ma, and J. Chen, "Improved interrupted sampling repeater jamming based on DRFM," in *Proceedings of the 2014 IEEE International Conference on Signal Processing, Communications and Computing (ICSPCC)*, pp. 254–257, Guilin, China, August 2014.

[12] H. Yuan, C. Wang, X. Li, and L. An, "A method against interrupted-sampling repeater jamming based on energy function detection and band-pass filtering," *International Journal of Antennas and Propagations*, vol. 2017, no. 1, pp. 1–9, 2017.

[13] S. Gong, X. Wei, and X. Li, "ECCM scheme against interrupted sampling repeater jammer based on time-frequency analysis," *Journal of Systems Engineering and Electronics*, vol. 25, no. 6, pp. 996–1003, 2014.

[14] J. Chen, W. Wu, S. Xu, Z. Chen, and J. Zou, "Band pass filter design against interrupted-sampling repeater jamming based on time-frequency analysis," *IET Radar, Sonar & Navigation*, vol. 13, no. 10, pp. 1646–1654, 2019.

[15] C. Zhou, Q. Liu, and C. Hu, "Time-frequency analysis techniques for recognition and suppression of interrupted sampling repeater jamming," *Journal of Radars*, vol. 8, no. 1, pp. 100–106, 2019.

[16] C. Zhou, Q. Liu, and X. Chen, "Parameter estimation and suppression for DRFM based interrupted sampling repeater jammer," *IET Radar, Sonar & Navigation*, vol. 12, no. 1, pp. 56–63, 2017.

[17] X. Lu, J. Yang, C. Ma, H. Gu, and W. Su, "Wide-band interference mitigation algorithm for SAR based on time-varying filtering and sparse recovery," *Electronics Letters*, vol. 54, no. 3, pp. 165–167, 2018.

[18] H. Yuan, C. Wang, X. Li, and L. An, "ECCM scheme against interrupted-sampling repeater jamming based on compressed sensing signal reconstruction," *Xi Tong Gong Cheng Yu Dian Zi Ji Shu/Systems Engineering and Electronics*, vol. 40, no. 4, pp. 717–725, 2018, Chinese.

[19] R. Shen, Z. Liu, J. Sui, and X. Wei, "Study on interrupted-sampling repeater jamming performance based on intra-pulse frequency coded signal," in *Proceedings of the Ninth International Conference on Digital Image Processing (ICDIP 2017)*, Hongkong, China, July 2017.

[20] J. Zhang and C. Zhou, "Interrupted sampling repeater jamming suppression method based on hybrid modulated radar signal," in *Proceedings of the 2019 IEEE International Conference on Signal, Information and Data Processing (ICSIDP)*, pp. 1–4, Chongqing, China, December 2019.

[21] W. Fan, F. Zhou, P. Rong, and X. Yao, "Interference mitigation for synthetic aperture radar based on deep residual network," *Remote Sensing*, vol. 11, no. 14, p. 1654, 2019.

[22] J. Rock, M. Toth, E. Messner, P. Meissner, and F. Pernkopf, "Complex signal denoising and interference mitigation for automotive radar using convolutional neural networks," in *Proceedings of the 2019 22th International Conference on Information Fusion (FUSION)*, pp. 1–8, Ottawa, Canada, July 2019.

[23] J. Yu, J. Li, B. Sun, J. Chen, and C. Li, "Multiclass radio frequency interference detection and suppression for SAR based on the single shot multibox detector," *Sensors*, vol. 18, no. 11, p. 4034, 2018.

[24] J. Chen, S. Xu, J. Zou, and Z. Chen, "Interrupted-sampling repeater jamming suppression based on stacked bidirectional gated recurrent unit network and infinite training," *IEEE Access*, vol. 7, pp. 107428–107437, 2019.

[25] J. Hu and W. Zheng, "A deep learning model to effectively capture mutation information in multivariate time series prediction," *Knowledge-Based Systems*, vol. 203, Article ID 106139, 2020.